LANGMUIR

pubs.acs.org/Langmuir Article

Quantification of Poly(ethylene glycol) Crowding on Nanodiamonds toward Quantum Biosensor for Improved Prevention Effects on Protein Adsorption and Lung Accumulation

Kazuaki Rikiyama, Nanami Maehara, Hiroshi Abe, Yushi Nishimura, Hiroshi Yukawa, Kiichi Kaminaga, Ryuji Igarashi, and Kensuke Osada*

Cite This: https://doi.org/10.1021/acs.langmuir.3c03988 Read Online

ACCESS | Metrics & More | Article Recommendations | Supporting Information

ABSTRACT: Nanometer-sized diamonds (NDs) containing nitrogen vacancy centers have garnered significant attention as potential quantum sensors for reading various types of physicochemical information *in vitro* and *in vivo*. However, NDs intrinsically aggregate when placed in biological environments, hampering their sensing capacities. To address this issue, the grafting of hydrophilic polymers onto the surface of NDs has been demonstrated considering their excellent ability to prevent protein adsorption. To this end, crowding of the grafted chains plays a crucial role because it is directly associated with the antiadsorption effect of proteins; however, its quantitative evaluation has not been reported previously. In this study, we graft poly(ethylene glycol) (PEG) with various molecular weights onto NDs, determine their crowding using a gas adsorption technique, and disclose the cross-correlation between the pH in the grafting reaction, crowding density, molecular weight, and the prevention effect on protein adsorption. PEG-grafted NDs exhibit a pronounced effect on the prevention of lung accumulation after intravenous injection in mice. PEG crowding was compared to that calculated by using a diameter determined by dynamic light scattering (DLS) assuming a sphere.

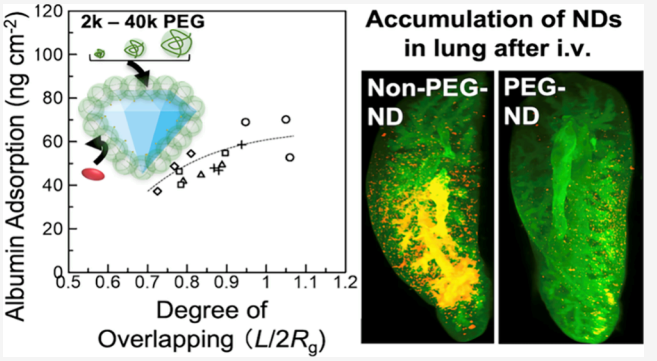

INTRODUCTION

Nanometer-sized diamonds (NDs) containing nitrogen vacancy (NV) centers have garnered significant interest as potential quantum biosensors for reading physicochemical information not only *in vitro* but also *in vivo*.[1−7] NDs with NV centers emit near-infrared fluorescence, which can penetrate deep in tissue through a biological window (650 to 1350 nm), do not undergo photobleaching or blinking in contrast to conventional organic fluorescent reagents, and do not undergo chemical reactions with biological substances because of their extremely high chemical stability.[8,9] Moreover, fluorescence changes depend on the ambient environment, such as temperature, pH, magnetic field, and electric field, which can be distinguished through a quantum technique of optically detected magnetic resonance (ODMR)[10,11] and some other pulsing schemes,[12−14] permitting great utility in probing local information. Despite these appealing properties, NDs readily interact with biological substances, including proteins, when placed in the physiological environment, resulting in agglomeration.[15−18] Aggregation interferes with intrinsic local metabolism and ultimately the maintenance of the homeostasis of the host. Furthermore, it discourages steady blood circulation when injected into the bloodstream because it provokes nonspecific interactions with serum components and blood vessels and may result in embolization or even rupture of blood vessels. Thus, the prevention of nonspecific interactions with biological substances is a primary prerequisite for biosensing. Ideally, NDs should localize stealthily in the host environment without being recognized for long periods. Modifying the surfaces of NDs with hydrophilic polymers has been acknowledged as effective in appending such stealth properties to NDs.[19−22] In this respect, NDs have often been modified with hydrophilic neutral polymers with linear or hyperbranched form, or twitterionic polymers, and subjected to *in vitro* and *in vivo* applications.[23−27] However, quantitative information concerning the crowding of polymers grafted onto NDs has not been previously reported. Crowding is essential for preparing stealth NDs because it not only provides information on the conformation and thickness of the polymer chains grafted on the surface of the NDs but also directly

Received: December 24, 2023
Revised: April 5, 2024
Accepted: April 9, 2024

affects the capability of the antiadsorption effect against proteins.[28,29] The determination of crowding is actually challenging because accurate estimation of the surface area of the NDs, which is a necessary factor to calculate the grafting density and, thereby, the crowding, is difficult. The surface area is often calculated from the radius of the nanoparticles measured from electron microscopy (EM) images. This is possible for spherical nanoparticles; however, the geometry of NDs was much complicated deviated from sphere, including flake-like and rod-like geometry depending on manufacturers.[30−32] The hydrodynamic radius (R_h) determined by dynamic light scattering (DLS) measurement is occasionally used as the radius of the nanoparticles; however, it is the apparent radius of a nanoparticle assumed to be a rigid sphere and thus does not provide an accurate surface area of NDs.

To address these issues, we grafted polymers onto NDs, determined their density using a gas adsorption method, and quantified crowding in terms of the degree of chain overlap with adjacent chains. The grafting was employed by a most typical method with an aim of gaining insight into the extent of crowding and their protein adsorption inhibitory effect achievable by that method, that is, grafting the most representative biocompatible polymer, poly(ethylene glycol) (PEG), with a series of commercially available molecular weights, by the "grafting to" method with conventional condensation chemistry in water. We disclosed the cross-correlation between pH in the grafting reaction, crowding density, molecular weight, and antiadsorption effect of albumin and demonstrated a pronounced effect of PEG grafting on accumulation in the lungs after intravenous injection in mice. Last, PEG crowding was also calculated using a diameter determined by dynamic light scattering (DLS) assuming a sphere, highlighting the gas adsorption method as a more relevant technique to estimate the surface area and thereby the grafting density.

MATERIALS AND METHODS

Materials. NDs with a nominal particle size of 50 nm (MD-50, pristine NDs, nonfluorescent) were purchased from Tomei Diamond Co., Ltd. (Tochigi, Japan). Sulfuric acid, nitric acid, sodium hydroxide, sodium chloride, dimethyl sulfoxide (DMSO), fluorescamine, 1,6-diaminohexane, and butylamine were purchased from FUJIFILM Wako Pure Chemical Co. (Osaka, Japan). *N*-Hydroxysuccinimide (NHS) was purchased from Sigma-Aldrich (St. Louis, MO, USA). Bovine serum albumin (BSA) was purchased from Nacalai Tesque (Kyoto, Japan). The condensation reagent 1-ethyl-3-(3-(dimethylamino)propyl) carbodiimide hydrochloride (EDC) was purchased from Dojindo (Kumamoto, Japan). α-Methoxy-ω-amino-PEGs (PEG-NH_2, M_n = 2000, 5000, 12000, 20000, 40000) were purchased from NOF (Tokyo, Japan). All of the reagents were used as purchased. Amino-functionalized cyanine 5 (Cy5-NH_2, Funakoshi Co., Ltd., Tokyo, Japan) was dissolved in DMSO and used as a 5 mg/mL stock solution.

Methods. *Preparation of ND-COOH.* Pristine NDs were placed in an electric furnace (ROP-100P, AS ONE Co., Japan) at 535 °C for 2 h under air for oxidation. The heat-treated NDs were added in a mixture of H_2SO_4 and HNO_3 (3:1 v/v, 100 mg/mL) and sonicated using ultrasonic bath (Bioruptor II, Sonicbio Co., Ltd., Kanagawa, Japan) (on/off = 30 s/90 s, 99 cycles). The suspension was stirred on a hot stirrer at 330 °C for 1 h and allowed to stand overnight at room temperature. The supernatant was thereafter removed by decantation. The residue was aliquoted into conical tubes, diluted with water, resuspended in a sonicator, and centrifuged to precipitate NDs (Model 3740, Kubota Co., Tokyo, Japan). This purification process was repeated, until the pH of the supernatant was neutral. After resuspension in water, the sample was lyophilized to obtain the ND-COOH powder.

Quantification of Carboxy Group on ND-COOH. NHS, EDC, and 1,6-diaminohexane were added to an aqueous suspension of ND-COOH. The suspension was sonicated and stirred at 50 °C overnight to conjugate 1,6-diaminohexane to ND-COOH and introduce NH_2 groups onto the NDs. NHS and EDC were added twice during the reaction. The reaction mixture was diluted with water, sonicated, and centrifuged to precipitate NDs from the unreacted reagents in the supernatant. This washing process was repeated thrice for purification. The NDs were thereafter resuspended in water and lyophilized to obtain ND-NH_2. ND-NH_2 was suspended in DMSO and incubated with fluorescamine for 3 h. The fluorescence spectra were measured using a fluorescence spectrophotometer (FP-8600, JASCO Co., Tokyo, Japan) to determine the number of amino groups on the NDs, which is termed the number of carboxyl groups available. A calibration curve was prepared using butylamine as the standard compound with fluorescamine in DMSO.

Grafting of PEGs to ND-COOH. NHS, EDC, and PEG-NH_2 were added to a suspension of ND-COOH in water. The mixed suspension was sonicated and stirred overnight at 50 °C on a hot stirrer for condensation reaction; meanwhile, the NHS and EDC were added twice. The PEG concentration in the reaction suspension was set to twice the overlapping concentration (C^*) of each molecular weight. The HCl solution was added to the suspension to adjust the pH to 7 and 4. After the reaction, the suspension was diluted with water and centrifuged to remove the unreacted substances and the supernatant. This process was repeated three times to purify the product. The product was thereafter dispersed in water, sonicated, and lyophilized to obtain ND-PEGs. The hydrodynamic diameters and zeta potential of the ND-PEGs in water were measured using a Zetasizer Nano ZS (Malvern Panalytical Ltd., Malvern, UK) at 0.1 mg/mL. Prior to the measurement, the sample dispersion was sonicated and filtered by a 0.45 μm syringe filter to remove dust.

Determination of PEG Grafting Density to NDs. The PEG grafting density, σ (chains/nm^2), on the ND surface was calculated from the weight of the grafted PEG and the specific surface area of the NDs. The weight of PEG was determined from the weight loss due to thermal decomposition by using a thermogravimetric analyzer (TGA-50, SHIMADZU, Kyoto, Japan) under a nitrogen atmosphere. The NDs were dispersed in water, sonicated, lyophilized, and used for measurements. The weight loss from 200 to 450 °C was considered to be the amount of grafted PEG. The weight was converted to the number of PEG chains per 1 g of NDs. The specific surface areas of the NDs were determined by the Brunauer−Emmett−Teller (BET) method from the adsorption isotherm of N_2 gas using a TriStar 3020 specific surface area analyzer (Micromeritics, GA). The lyophilized NDs were treated in a VacPrep 061 degasser (Micromeritics, GA) at 200 °C for 3 h in vacuo before the measurement. The distance between adjacent tethered PEG chains, L (nm), was obtained as the square root of σ. The radius of gyration (R_g) of PEGs, defined as the average of the distance between the monomer units in the polymer segment and the center of gravity in the random coil conformation, was calculated as R_g = 0.181 × (number of monomer unit)$^{0.58}$ (nm).[29,33,34] The PEG crowding density was obtained as $L/2R_g$ and the reduced tethering density (RTD) was calculated as $\sigma\pi R_g^2$.

BSA Adsorption on NDs. BSA was dissolved in HEPES buffer containing NaCl at physiological concentrations (HEPES 10 mM, NaCl 150 mM, pH 7.4) of 2 mg/mL. Pristine NDs and ND-PEGs were added to HEPES buffer (HEPES 10 mM, NaCl 150 mM, pH 7.4) at 20 mg/mL and sonicated. Equal volumes of BSA solution and NDs suspension were mixed (NDs: 10 mg/mL, BSA: 1 mg/mL) and incubated at 37 °C for 5 h to allow for the adsorption of BSA on NDs. The NDs in the mixture were precipitated by centrifugation, and the amount of BSA remaining in the supernatant was determined by a Pierce BCA protein assay kit (Thermo Fisher Scientific, Waltham, MA) using an ultraviolet−visible spectrophotometer (V-560, JASCO Co., Tokyo, Japan). The amount of BSA adsorbed onto the NDs was determined by subtracting the amount of BSA in the supernatant from the total amount used for the measurement.

https://doi.org/10.1021/acs.langmuir.3c03988
Langmuir XXXX, XXX, XXX−XXX

Table 1. Quantification of PEG crowding grafted onto NDs reacted at various pH conditions

PEG MW	Rg (nm)	number of PEG (chains/g ND)			σ (chains/nm^2)			$L/2R_g$			RTD		
		pH 10−11	pH 7	pH 4	pH 10−11	pH 7	pH 4	pH 10−11	pH 7	pH 4	pH 10−11	pH 7	pH 4
2000	1.6	7.34×10^{18}	7.46×10^{18}	9.24×10^{18}	0.0864	0.0878	0.109	1.06	1.05	0.948	0.695	0.706	0.874
5000	2.8	3.60×10^{18}	3.08×10^{18}	3.50×10^{18}	0.0423	0.0362	0.0412	0.868	0.938	0.880	1.04	0.893	1.02
12000	4.6	1.61×10^{18}	1.27×10^{17}	1.44×10^{18}	0.0289	0.0150	0.0169	0.790	0.888	0.835	1.26	0.997	1.13
20000	6.2	9.09×10^{17}	6.89×10^{17}	9.00×10^{17}	0.0107	0.00811	0.0106	0.780	0.896	0.784	1.29	0.979	1.28
40000	9.3	4.68×10^{17}	3.75×10^{17}	4.17×10^{17}	0.00551	0.00441	0.00491	0.725	0.810	0.768	1.50	1.20	1.33

Scheme 1. Reaction Schemes of PEG Grafting (a) and the Introduction of an Amino Group (b) to NDs by Condensation

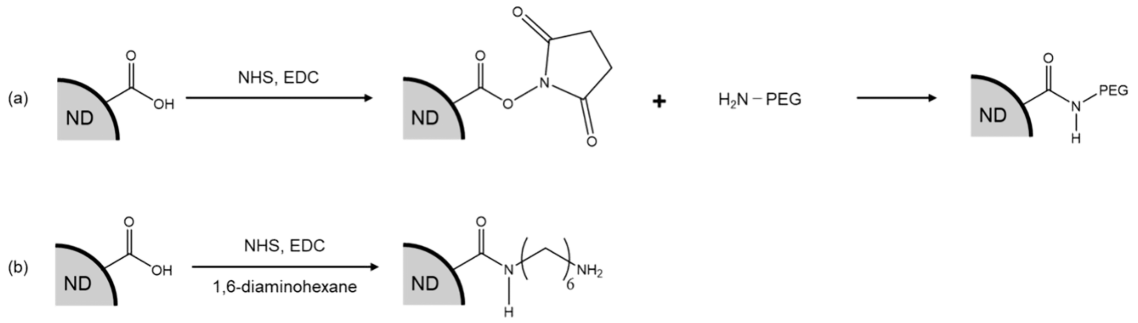

Lung Accumulation of NDs. The animal experimental protocol was approved by the Animal Care and Use Committee of the National Institutes for Quantum Science and Technology, Japan. All animal experiments were conducted in accordance with the guidelines for animal care and handling. ND-COOH and ND-PEG20k were labeled with Cy5, respectively. Briefly, NHS, EDC, and Cy5-NH_2 with 5, 2, and 2 equiv, respectively, to the amount of carboxyl group estimated was added to a suspension of ND-COOH or ND-PEG20k in water. The suspension was sonicated and stirred overnight at room temperature for a condensation reaction. After the reaction, the suspension was diluted with water and centrifuged to remove the unreacted substances and the supernatant. This process was repeated thrice to purify the product. The product was dispersed in water, sonicated, and lyophilized to obtain the Cy5-labeled NDs. The Cy5-labeled NDs were suspended in PBS (1 mg/mL) and sonicated. The suspension of 200 μL was vortexed and injected to tail veins of C57 BL/6 JJms Slc mice (female, 9 weeks old). The mice were perfused with saline containing heparin 5 min postinjection and sacrificed, and their lungs were excised (n = 5). The lungs were homogenized in lysis buffer (Passive Lysis 5 X buffer, Promega, Madison, WI, USA) containing 1% Triton X-100 using a handy homogenizer. The lysed solution was dispensed into a 96-well plate, and Cy5 fluorescence was measured using an Infinite M200 PRO spectrophotometer (Tecan Group Ltd., Männedorf, Switzerland). The fluorescence intensities of homogenized lung samples from mice treated with PBS without NDs were measured as a background and subtracted from those of mice treated with NDs. The concentration of ND-COOH and ND-PEG20k labeled with Cy5 in lungs were determined from the standard curves prepared for each ND in PBS suspensions and normalized by the weight of lung received ND-COOH and ND-PEG20k injection, respectively. The p values were determined by Student's t test using a one-tailed distribution and two-sample equal variance with the t test function in Microsoft Excel. The p values of less than 0.05 were considered statistically significant.

For the study of cleared lungs, the mice received the same protocol as described, and their lungs were excised 1 h postinjection. The lungs were fixed in 4% PFA−PBS for 1 d, washed in PBS with shaking for 2 h thrice by refreshing the PBS, immersed in CUBIC-L, the chemical cocktail for delipidation and decoloring, and incubated for 6 days at 37 °C with gentle shaking. The CUBIC-L solution was refreshed three times during this process. The lungs were washed by shaking in PBS for 2 h, and the PBS was refreshed. This process was repeated thrice. The lungs were immersed into the staining solution containing 1% of the α-smooth muscle actin FITC-conjugated antibody (catalog no. F3777, Sigma, St. Louis, MO) and 0.25% of the Blocker Casein (Thermo Fisher Scientific, Waltham, MA) in PBS for 5 days at room temperature for staining vessels. The stained lungs were washed with PBS and immersed in 50% CUBIC-R aqueous solution, the chemical reagent for refractive index (RI) matching, with gentle shaking at room temperature for 1 day. The lungs were washed with PBS and immersed in 100% CUBIC-R solution with shaking at room temperature for 1 day to complete the RI-matching process.[35] The cleared lungs were observed using a light-sheet microscope (Ultra-Microscope II, Miltenyi BioTec, Bergisch Gladbach, Germany), and images were processed using an Imaris (Ver 9.9.0, Oxford Instruments, Abingdon, UK). The threshold for distinguishing the NDs from the background was determined using Fiji (ImageJ), a freely available software for processing and analyzing images (version 1.54b).[36] A total of 10 arbitrary slices among the slices of the light-sheet microscopy images of the lungs were taken, and three 100 × 100 pixel regions, which did not include apparent bright spots considered as NDs, were collected from each of the slices. The maximum signal intensity of these 30 regions was set as the background intensity, and intensities above this threshold were defined as NDs. For quantification, the intensities of each pixel above the threshold were summed for all slices and normalized to the weight of the lungs and the fluorescence intensity of Cy5 per gram for ND-COOH and ND-PEG, respectively.

RESULTS AND DISCUSSION

PEG grafting onto NDs was performed as follows: the purchased NDs (pristine NDs) were heat-treated in air followed by acid treatment to prepare carboxyl group-introduced NDs (ND-COOH). The carboxyl groups on NDs were activated with EDC and NHS, and reacted with α-methoxy-ω-amino-PEG (PEG-NH_2) with different molecular weights (Table 1) in water to obtain a series of ND-PEGs (Scheme 1a). Details of each process are given in the following sections.

(i). Preparation of ND-COOH. The pristine NDs were annealed for air oxidization such that impurities, including sp^2 carbons attached to the surface of the NDs, would be removed, and oxygen species, including hydroxy groups, ketones, and aldehydes, would be introduced onto the surface.[8] The NDs

https://doi.org/10.1021/acs.langmuir.3c03988
Langmuir XXXX, XXX, XXX−XXX

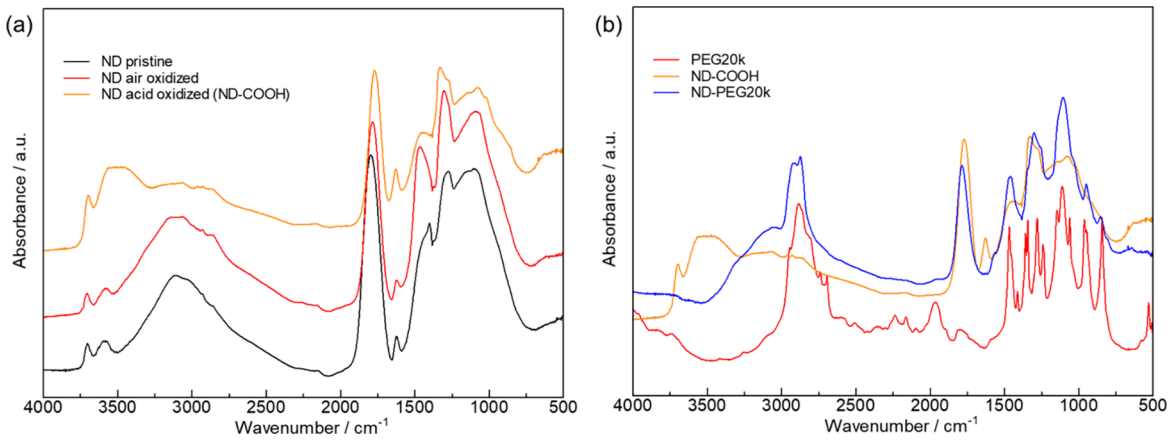

Figure 1. IR spectra of NDs in the processes of (a) oxidization and (b) PEG grafting in the as-reacted condition.

were thereafter treated in a boiling solution of nitric and sulfuric acids to oxidize the oxygen species into carboxyl groups.[37,38] The processed NDs were characterized by using Fourier-transform infrared (FT-IR) spectroscopy (Figure 1a). The peak at approximately 1700−1800 cm^{-1} was assigned to stretching vibrations of the C═O double bond, which includes esters, aldehydes, ketones, carboxylic acids, and acid anhydrides.[37] The O−H stretching vibrations were included in the broad peaks at 2000−3800 cm^{-1}.[39] It is expected that the peak area ratio $A_{2000-3800}/A_{1700-1800}$ increases if the acid treatment converts the oxygen species to a carboxyl group. The increased ratio upon acid treatment is in good agreement with the successful introduction of carboxyl groups on the NDs (Table 2). The negative shift in the zeta potential is also in good agreement with the introduction of carboxyl groups on the NDs (Table S1).

Table 2. Peak Area and the Ratio between the Carbonyl Group and Hydroxy Group in IR Spectra

	$A_{1700-1800}$	$A_{2000-3800}$	$A_{2000-3800}/A_{1700-1800}$
ND pristine	14.1	37.0	2.63
ND air oxidized	11.9	56.7	4.77
ND acid oxidized	11.5	69.9	6.07

(ii). Quantification of Carboxyl Groups on ND-COOH Available for Condensation. Prior to the subsequent condensation reaction between ND-COOH and PEG-NH_2 to prepare ND-PEGs, it was important to evaluate whether the density of the carboxyl groups on the surface of ND-COOH was sufficient to fully coat the surface with PEG. However, it is difficult to directly quantify the carboxyl groups on NDs. Thus, we introduced a low-molecular-weight compound of 1,6-diaminohexane by the condensation reaction (Scheme 1b) and quantified the amino group of the other terminal using fluorescamine, a reagent widely used to determine the amount of primary amino groups as carboxy groups available for the condensation reaction, which was determined to be 22 μmol per 1 g of ND. Subsequently, we employed TEM to determine the surface area of the NDs and found that the shapes of the NDs deviated from spherical (Figure S1), which was consistent with the individual particle analyses based on SEM.[31] Therefore, we excluded measuring the diameter to calculate the surface area under the assumption of a sphere. An alternative method is to use the hydrodynamic radius (R_h) determined from DLS measurements, which is sometimes used to calculate the surface area. However, we consider this option risky because R_h is numerically calculated from the diffusion constant of a particle assuming a rigid sphere with that radius and this assumption conflicts with the shape of the NDs. Finally, we employed a N_2 gas adsorption isotherm with BET analysis to obtain the specific surface area of the NDs, which was determined to be 85 m^2/g. Thus, the density of the available carboxyl groups on the surface of ND-COOH was estimated to be 0.16/nm^2, indicating one site in the lattice with a side length of 2.5 nm square. The unit lattices were compared with the R_g values of the PEGs (Table 1). The lattice size is smaller than the gyration diameter of the PEGs used for grafting (Figure S2), indicating that the carboxyl groups were sufficient to cover the surface of the NDs with PEG when the subsequent condensation reaction proceeded quantitatively.

(iii). PEG Grafting onto NDs. The grafting of PEGs onto the NDs was performed in a one-pot reaction of ND-COOH, PEG-NH_2, EDC, and NHS in water. The PEG concentration was set at twice the overlapping concentration (C^*) of each molecular weight (Table S2). The reaction comprises two steps: introduction of the NHS group to the carboxyl group of the NDs to form activated ester groups catalyzed by EDC followed by the addition of PEG−NH_2 to the activated ester groups for condensation. It is acknowledged that the first- and second-step reactions proceed preferentially under acidic and neutral to basic conditions, respectively.[40,41] The reaction suspensions were basic (pH 10−11) because of the presence of the amino group in PEG−NH_2 (Table S2), which may have affected the efficiency of the first step of the reaction. In this respect, the reaction was performed not only in the as-reacted suspension (without pH adjustment) but also in the suspensions adjusted to pH 7 and 4. The PEG-grafting process was investigated by using FT-IR spectroscopy. The characteristic peaks of PEG derived from C−H stretching vibration in the CH_2 group (around 2900 cm^{-1}) and C−O−C vibrations of the ether group (1150−1070 cm^{-1}) appeared in the spectrum of ND-PEG20k (Figure 1b, as a representative demonstration), indicating the success of the PEG grafting. The quantity of PEG grafted onto ND-PEG was determined by TG under a nitrogen atmosphere. The weight decrease between 200 and 450 °C in the TG profile of ND-PEGs was assigned as the quantity of PEG grafted (Figure 2, Figure S4). Here, the following reasons were considered in the assignment: PEG had completed the thermal decomposition by 450 °C

https://doi.org/10.1021/acs.langmuir.3c03988
Langmuir XXXX, XXX, XXX−XXX

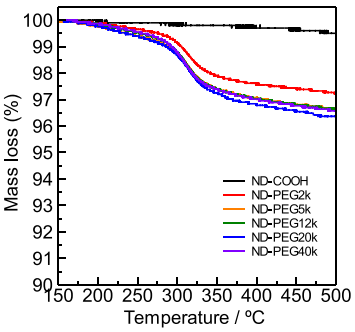

Figure 2. Thermogravimetric analysis traces of ND-PEGs prepared in the as-reacted condition. The weight at 150 °C was set to 100%.

(Figure S3), ND-COOH did not exhibit any noticeable weight loss until 450 °C (Figure S3), organic impurities attached to the NDs had already been removed because the ND-PEGs underwent thermal treatment at 515 °C prior to the PEG grafting reaction, and the water that possibly remained in the ND-PEG samples was assumed to evaporate until 200 °C. The effect of thermal drift was also considered when analyzing the profile. The quantification showed that the grafting reaction proceeded successfully under any pH condition and that the lower the PEG molecular weight, the more PEG chains were grafted onto the NDs (Table 1).

The hydrodynamic size of the ND-PEGs determined by DLS showed monodispersed sub-100 nm-sized particles in water (Figure 3, Figure S5). The profiles exhibited a slight shift

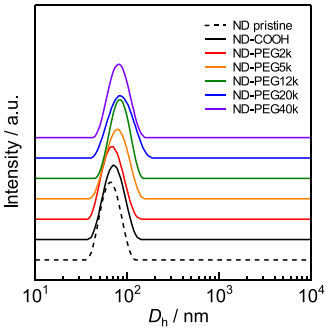

Figure 3. Intensity profiles of D_h determined by DLS for NDs grafted with various PEGs prepared in the as-reacted condition.

in size after PEG grafting, which was not as apparent as the molecular weight of the grafted PEGs. Notably, the hydrodynamic size was determined from the diffusion rate of the particles in solution, and the density of diamonds is exceedingly higher than that of PEG (diamond 3.52 g/cm^3 and water-containing PEG 1−1.1 g/cm^3), demonstrating that the diffusion of the ND-PEGs is mainly dominated by the NDs. Thus, it is expected that the presence of a PEG layer has a small impact on the diffusion rate, resulting in an insignificant effect on the size of the ND-PEGs measured by DLS. The zeta potential of NDs slightly shifted to positive after the PEG grafting, although some of those reacted at pH 7 were not significant (Table S1).

(iv). Crowding PEG Grafted onto NDs. Since the quantity of PEG grafted to NDs and the specific surface area were obtained, along with the confirmation that ND-PEGs are monodisperse in water, the density of PEG on NDs was calculated as chains/nm^2 (σ, Table 1). The density depended on the molecular weight of the PEG used, with lower molecular weights being higher. However, this value does not intuitively indicate the crowding of the PEG chains on the ND surface. Crowding is an important factor in preventing protein adsorption.[29,42,43] Therefore, $L/2R_g$ was calculated by normalizing the distance between adjacent PEG chains (L) to the diameter of the gyration of the PEG chain ($2R_g$) as an index to represent the degree of crowding. This value indicates the degree of chain overlap between adjacent chains and allows for a comparison of crowding between different molecular weights because the molecular weight factor is included in R_g. $L/2R_g$ = 1 indicates that the PEG chains are in adjacent contact, >1 indicates that the PEG chains are separated from each other, and <1 indicates that the adjacent PEG chains overlap, indicating that the lower the $L/2R_g$ value, the more densely grafted they are (Scheme 2). It was found that the $L/2R_g$ values were generally less than 1, except for ND-PEG2k, which reacted at pH 7 under basic conditions (Table 1). Furthermore, crowding showed a correlation with the logarithm of the molecular weight of the PEGs (Figure 4),

Scheme 2. Schematic Illustrations of PEG Crowding on the Surface in $L/2R_g$

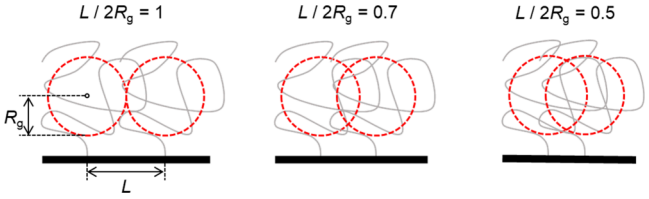

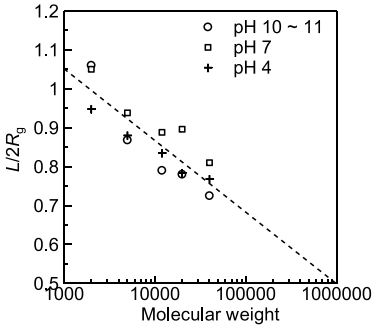

Figure 4. PEG crowding on NDs as a function of PEG molecular weight. The dotted line was determined from the linear least-squares method.

with the trend that the larger the molecular weight of PEG used, the more overlapped the grafting was achieved. It was also found that more crowding of PEGs was achieved when reacting under basic or acidic conditions than under neutral conditions.

(v). Effect of PEG Crowding on the Prevention of BSA Adsorption by NDs. Having determined the degree of PEG crowding on the NDs, the effect on the prevention of protein adsorption to the NDs was evaluated. BSA was used as a representative protein because it is present at the highest concentration among all proteins in the blood. The pristine NDs received an adsorption of BSA with a concentration of 118 ng/cm^2. In contrast, the PEG-grafted NDs exhibited significantly lower adsorption (Figure 5), confirming the preventive effect of PEG grafting. It was observed that the

https://doi.org/10.1021/acs.langmuir.3c03988
Langmuir XXXX, XXX, XXX−XXX

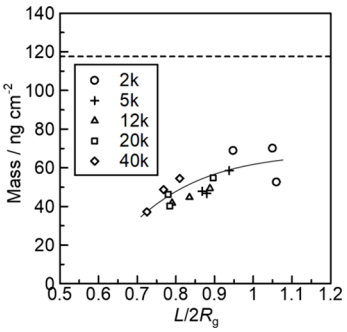

Figure 5. BSA adsorption on PEG grafted NDs as a function of PEG crowding. The solid line is a guide for eye and the dotted line is the mass of BSA adsorbed on pristine NDs.

ND-PEGs grafted with higher molecular weights had better preventive effects. In particular, the quantity of adsorbed BSA correlated with $L/2R_g$, with the smaller, alternatively, the greater the overlap between adjacent PEG chains, the higher the preventive effect, corroborating the substantial role of crowding in preventing BSA adsorption.

(vi). Effect of PEG Grafting on Lung Accumulation. Encouraged by the significant effect of PEG grafting on the prevention of BSA adsorption, NDs were intravenously injected into mice. Various blood components, including serum proteins, are readily adsorbed onto particles when injected into the blood, resulting in their agglomeration. The lungs are an organ in which aggregates are prone to accumulation and embolization. Therefore, we focused on lung accumulation to evaluate the effect of PEG grafting. ND-COOH and ND-PEG20k, representative ND-PEGs, were labeled with Cy5 and injected into the tail vein. ND-COOH has been considered to have high biocompatibility *in vivo*; therefore, it was used as a positive control in this evaluation.[44] The concentrations of ND-COOH and ND-PEG20k labeled with Cy5 in homogenized lungs were determined from their standard curves (Figure S6) and normalized by the weight of lungs, respectively. Significant amounts of ND-COOH accumulated in the lungs (Figure 6a), suggesting that aggregation occurred in the blood. In contrast, ND-PEG exhibited significantly lower accumulation. To determine the location of accumulation, the lungs were subjected to tissue clearing by CUBIC treatment[35] and observed under a light-sheet microscope. First, the quantification of Cy5 signals from the images showed a significantly lower accumulation of ND-PEG than that of ND-COOH (Figure 6b), which is consistent with the quantification from the homogenized samples (Figure 6a). Transmission images of the entire lungs revealed the accumulation of NDs (Figure 6c; see the supporting movies for the rotation). Intense signals (yellow) were observed along the lung artery for ND-COOH (Figure 6c(i)), in contrast to those for ND-PEG (Figure 6c(ii)). A section slice of the lung artery revealed that ND-COOH was localized along the vessel wall (Figure 6d(i)). Considering that the intravenously injected NDs first reached the heart and then the lung, ND-COOH was adsorbed to the vessel wall of the artery when entering the lung, possibly in the first pass. Furthermore, a pattern of widespread Cy5 signals was observed in the lower part of the lung for ND-COOH (Figure 6c(i), Supporting Movie). The sections showed that the signals were three-dimensionally distributed in the lung tissue (Figure 6e), suggesting bleeding. It is likely that ND-COOH clogged the vessels. In contrast, this spread pattern was not apparent for ND-PEG (Figure 6c(ii)). Small red spots were observed throughout the lungs for both NDs, with fewer spots for ND-PEG than for ND-COOH (Figure 6c). The section at the periphery of the lung showed colocalization of ND-COOH and capillaries (Figure 6f,

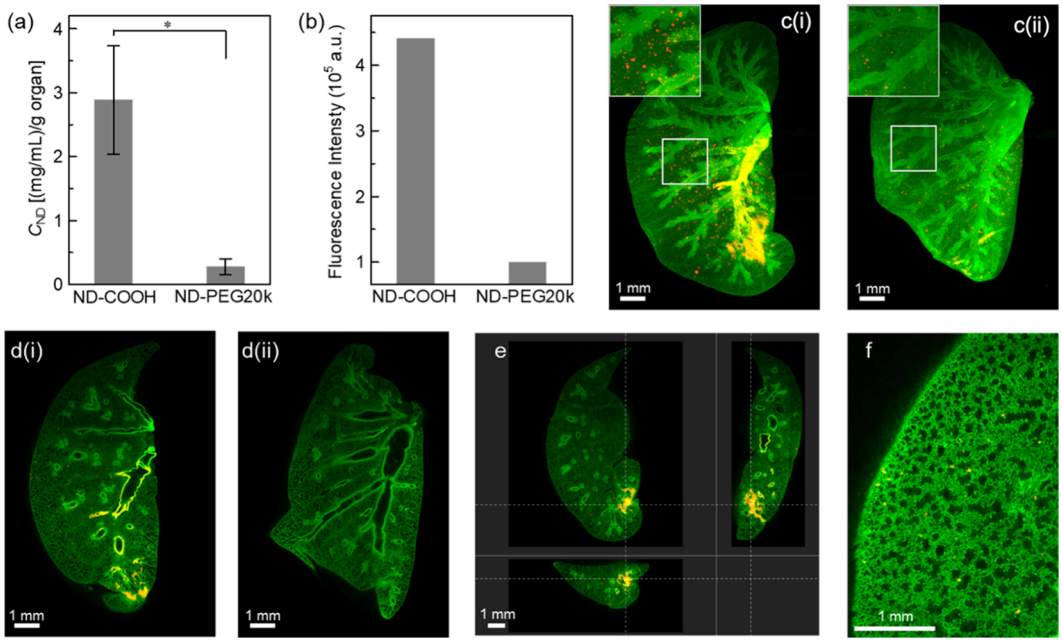

Figure 6. Accumulation of Cy5-labeled NDs at lungs after intravenous injection. Quantifications from the homogenized tissues (a) and from the images of the light sheet microscope in the cleared lungs (b). (c) Transmission images of cleared lungs received ND-COOH (i) and ND-PEG20k (ii) with magnified images in inset. NDs and blood vessels are shown in red and green, respectively. (d) Sections at the lung artery received ND-COOH (i)) and ND-PEG20k (ii). (e) 3-plane sections at the bleeding region received ND-COOH. (f) Section at the periphery of the lung received ND-COOH.

https://doi.org/10.1021/acs.langmuir.3c03988
Langmuir XXXX, XXX, XXX−XXX

yellow), suggesting embolization. Overall, the significant effect of PEG grafting onto the NDs was verified when preventing of lung accumulation.

Overall, we grafted PEG onto the ND surface by using a typical method and determined its crowding. This quantitative study allowed for verification of the following five issues:

First, NDs grafted with higher PEG crowding can be obtained by performing a condensation reaction under basic or acidic conditions instead of under neutral conditions (Figure 4). In the two-step condensation reaction, acidic conditions are favorable for the first step, and neutral to basic conditions are favorable for the second step. The pH of the as-reacted PEG solution was basic ranging from 9.5 to 11.2 owing to the presence of an amino group in PEG−NH_2 (Table S2). Therefore, there was concern that the first step of the reaction would not proceed well under basic as-reacted conditions. From this perspective, we adjusted the pH to acidic or neutral values to determine the optimal conditions for the condensation reaction. The quantification revealed that PEG crowding was even higher for ND-PEGs prepared under the as-reacted conditions than for those prepared at pH 7. PEG crowding performed under acidic conditions was also higher than that at pH 7, despite the unfavorable conditions for the second step of the reaction. It is presumed that the promotion of the second-step reaction in a basic environment compensates for the unfavorable first-step reaction and the promotion of the first-step reaction in a pH 4 environment compensates for the unfavorable second-step reaction. In contrast, neither process might be promoted at pH 7, resulting in the lowest level of PEG crowding. Notably, the $L/2R_g$ value for PEG2k under the as-reacted conditions was higher than that expected from the trend of other molecular weights in the molecular-weight dependence of $L/2R_g$ (Figure 4). The PEG2k solution contained the highest molar concentration of amino groups among the other series because the PEG concentration was set to $2C^*$ in all of the reactions, giving rise to the highest pH (Table S2). Such a high pH may limit the first-step reaction more than the promotion of the second-step reaction could compensate.[41]

Second, the PEG modification method used in this study yielded NDs entirely covered by PEG because the $L/2R_g$ values were verified to be less than 1, except for ND-PEG2k, which reacted at pH 7 or without pH adjustment (Figure 4).

Third, PEG crowding is dependent on the molecular weight of the PEG used; the larger the molecular weight of the PEGs, the more overlapping modifications of chains can be obtained. Several factors may be involved in this dependence on the molecular weight. First, the interactive potency between the PEG chains may be a factor. Interactive potency is expressed by the second virial coefficient A_2, where a positive value indicates that the chains are more repulsive, whereas a negative value indicates that they are more attractive. A_2 of PEG in water is positive and depends on the molecular weight; the higher the molecular weight, the lower the A_2 (Figure S7).[45] This indicates that PEG with a higher molecular weight permits the overlapping of chains; alternatively, PEG2k with a higher A_2 compared with other PEGs tends to refuse overlapping. Next, the spatial density of PEG, that is, the mass of a chain in the volume occupied by a single chain, may also be relevant to molecular weight dependence. Given a sphere of PEG in a random coil conformation with R_g, the spatial density was lower for PEGs with higher molecular weights (Figure S8), for instance, the spatial density of PEG40k was 1/10 that of PEG2k. It is assumed that a lower spatial density permits more overlapping chains. Furthermore, the density of the activated carboxyl groups in the condensation reaction of NDs may also be a factor. It is ensured that the density was sufficient for grafting PEG with overlapping. However, the number of activated carboxyl groups per PEG chain was higher for higher molecular weight PEG than for lower molecular weight PEG (Figure S2), allowing PEG of higher molecular weight to more likely locate the reactive point than PEG of lower molecular weight. These factors may collectively affect the efficiency of PEG grafting, resulting in the molecular weight dependence of $L/2R_g$.

Fourth, quantification allowed us to infer the conformation of PEG and the height of the PEG layer (H) on the NDs. Unperturbed single PEG molecules tethered to the surface adopt a random coil conformation known as a mushroom, such that its conformational entropy is maximized. In this case, H was assumed to be equivalent to $2R_g$. The correlation between the grafting density and conformation has been discussed using a parameter of RTD ($\sigma/\pi R_g^2$), which refers to the number of tethered chains settled in the area πR_g^2 covered by a chain in an unperturbed conformation (Figure S9).[46−48] RTD < 1 indicates that the PEG chains do not overlap with neighboring PEG chains, RTD = 1 indicates the onset of overlap, and RTD = 2 indicates that two PEG chains are packed in the area of πR_g^2. With the RTD, tethered polymer chains can be assigned into four possible conformations; (1) isolated mushroom (RTD < 1),[46,47] (2) overlapping mushroom (1 ≤ RTD), (3) squeezed, and (4) scalable brush regime characterized by H scaling as $\sigma^{1/3}$. The boundary between the overlapping mushroom and squeezed conformations is reported to be approximately RTD = 3.7−3.8,[49] and that between the squeezed and scalable brush conformations is at least 6. It is addressed that the value of the critical RTD should be independent of the molecular weight and solvent and should be universal for tethered chains.[49] Thus, these critical values was applied to PEG chains grafted onto NDs. The highest RTD value in the series of ND-PEGs was calculated as 1.5 (Table 1), which assigns the PEG chains to overlapping mushroom conformations and the height to the $2R_g$ equivalent.

Fifth, the preventive effect on BSA adsorption correlated well with the $L/2R_g$ of PEG (Figure 5), corroborating the significant role of crowding in the prevention effect. By collecting the molecular weight dependence and $L/2R_g$ (Figure 4), a clear cross-correlation revealed that grafting with a larger molecular weight allowed more overlap of PEG chains and provided a higher preventive effect against albumin adsorption. A correlation between $L/2R_g$ and serum protein adsorption was previously reported for PEG-modified substrates.[29] It is shown that the adsorption mass of serum proteins decreases as the $L/2R_g$ decreases in the range of $L/2R_g$ = 1.5−0.5. Our results on NDs ($L/2R_g$ = 1.1−0.7) are in good agreement with this report.

In particular, the report predicted that the adsorption of serum proteins could be completely suppressed when $L/2R_g$ fell below 0.5.[29] Accordingly, stealth NDs that can prevent the adsorption of serum proteins on the surface may be attained by increasing PEG crowding to $L/2R_g$ < 0.5, and such NDs may circumvent embolization in blood vessels when administered systemically. There are several ways to promote PEG crowding, including further increasing the density of the carboxyl group for the condensation reaction with PEG−NH_2, increasing the reaction efficiency, and increasing the

https://doi.org/10.1021/acs.langmuir.3c03988
Langmuir XXXX, XXX, XXX−XXX

concentration of PEG−NH_2 in the reaction. As for the density of carboxyl groups, we performed thermal oxidation in air to introduce oxygen species followed by intense acid oxidation using a boiling mixed acid to convert them to carboxyl groups. This density was sufficient for PEG grafting. Regarding the reaction efficiency, we checked various solvents for good dispersibility of the NDs, including water, DMSO, *N*,*N*-dimethylformamide, acetone, acetonitrile, methanol, ethanol, tetrahydrofuran, dichloromethane, chloroform, and toluene, and selected water as the best solvent. NHS and EDC were added several times during the condensation reaction to compensate for possible hydrolysis of the activated ester group. Furthermore, the reaction was performed at different pH values in pursuit of optimal conditions. Concerning the PEG concentration in the reaction solution, we performed the reaction at 2C^* for each molecular weight of PEG. It is expected that PEG crowding on the NDs would be similar to that of the solution if the reaction proceeds preferably, that is, $L/2R_g$ is 0.5, which is twice the overlapping concentration. However, the crowding quantified was not as high as expected. Notably, it is reported that the grafting density was saturated and did not effectively increase even when the concentration of PEGs in the solution was increased above the overlapping concentration.[42,50] Given these reports, a PEG concentration of 2C^* was assumed to be sufficient. Considering these notes, the room for significant improvement in elevated crowding may be limited. Theoretically, it is challenging to achieve the crowding of $L/2R_g < 0.5$. To achieve this, after a uniform modification with $L/2R_g = 1$, a greater number of PEG chains must shunt the grafted PEG chains, access the surface of the NDs, and accomplish the grafting reaction. This interferes with the conformational freedom of the PEG chains, resulting in a reduction in conformational entropy. In contrast, the correlation between $L/2R_g$ and molecular weight indicates that PEG crowding of $L/2R_g < 0.5$ could be attained using PEG with a molecular weight higher than 1000 kDa from the extrapolation of the trend (Figure 4). This challenge is intriguing, although it requires the synthesis of such high molecular weight PEG−NH_2 as the highest molecular weight commercially available is 40 kDa. Taken together, we consider that the PEG crowding has reached almost the upper limit in the modification by the "grafting to" method using commercially available PEGs via conventional EDC/NHS chemistry in water.

We also calculated PEG crowding using a diameter determined by DLS (Z-average hydrodynamic diameter of 67 nm), assuming a sphere. Overall, the PEG crowding was higher than that calculated using the gas adsorption method (Table S3). The RTD of NDs with higher molecular weight PEG was above 3.7, indicating that the PEG chains were squeezed.[46−48] Considering the substantial entropy penalty in squeezed conformation, it is unlikely to consider that PEG chains attain such conformation by the "grafting to" method. Moreover, the $L/2R_g$ of ND-PEGs prepared under the preferred pH conditions was below 0.5, except for PEG2k, which corresponds to crowding that can completely prevent protein adsorption. Our evaluation proved the substantial role of PEG in preventing BSA adsorption; however, complete prevention was not achieved (Figure 5). Given these observations, the calculation of PEG crowding based on the DLS data is considered to be overestimated. In this regard, the gas adsorption method is a more relevant technique to characterize the surface properties of NDs modified with polymers.

CONCLUSIONS

We grafted PEGs with a series of molecular weights onto NDs using a typical method and determined crowding for the first time, to the best of our knowledge. The quantification revealed the extent of PEG crowding on NDs, cross-correlation between the pH in the grafting reaction, molecular weight of the grafted PEGs, preventive effect on BSA adsorption, and conformation and height, which remained unaddressed in the polymer modification of NDs. In particular, it was revealed that grafting with a higher molecular weight PEG afforded a better prevention effect on BSA adsorption, and the PEG-grafted NDs could significantly reduce their adsorption to large arteries and bleeding in the lungs after intravenous injection. PEG-grafted NDs with maximized PEG crowding will allow for biosensing with minimal interference due to aggregation; meanwhile, the presence or thickness of polymer layer on the sensitivity of sensing might be necessary to be investigated for finer sensing in the future.

ASSOCIATED CONTENT

Supporting Information

The Supporting Information is available free of charge at https://pubs.acs.org/doi/10.1021/acs.langmuir.3c03988.

Tables for zeta potential of NDs, overlapping concentration of PEG and quantified PEG crowding; figures for TEM, density of the reactive points, TG profiles, DLS, photostability test, and standard curves of NDs labeled with Cy5, A_2 values of PEG, spatial density of PEG in water, and schematic illustrations of RTD (PDF)

Movies of cleared lungs after IV administration of NDs (MP4, MP4)

AUTHOR INFORMATION

Corresponding Author

Kensuke Osada − *Institute for Quantum Medical Science and Institute for Quantum Life Science, National Institutes for Quantum Science and Technology (QST), Chiba 263-8555, Japan;* orcid.org/0000-0001-9557-6851; Email: osada.kensuke@qst.go.jp

Authors

Kazuaki Rikiyama − *Institute for Quantum Medical Science and Institute for Quantum Life Science, National Institutes for Quantum Science and Technology (QST), Chiba 263-8555, Japan*

Nanami Maehara − *Institute for Quantum Medical Science, National Institutes for Quantum Science and Technology (QST), Chiba 263-8555, Japan; Department of Chemical and Biological Sciences, Faculty of Science, Japan Women's University, Tokyo 112-8681, Japan*

Hiroshi Abe − *Foundational Quantum Technology Research Directorate, National Institutes for Quantum Science and Technology (QST), Takasaki, Gunma 370-1292, Japan*

Yushi Nishimura − *Institute for Quantum Life Science, National Institutes for Quantum Science and Technology (QST), Chiba 263-8555, Japan*

Hiroshi Yukawa − *Institute for Quantum Life Science, National Institutes for Quantum Science and Technology (QST), Chiba 263-8555, Japan; Department of Quantum*

https://doi.org/10.1021/acs.langmuir.3c03988
Langmuir XXXX, XXX, XXX−XXX

Life Science, Graduate School of Science, Chiba University, Chiba 263-8522, Japan

Kiichi Kaminaga − *Institute for Quantum Life Science, National Institutes for Quantum Science and Technology (QST), Chiba 263-8555, Japan*

Ryuji Igarashi − *Institute for Quantum Life Science, National Institutes for Quantum Science and Technology (QST), Chiba 263-8555, Japan;* orcid.org/0000-0003-4415-9702

Complete contact information is available at: https://pubs.acs.org/10.1021/acs.langmuir.3c03988

Notes

The authors declare no competing financial interest.

■ ACKNOWLEDGMENTS

This work was financially supported by MEXT Quantum Leap Flagship Program (MEXT Q-LEAP, Grant Number JPMXS0120330644) and MEXT Grants-in-Aid (Grant Number 17KK0102, 21H03832, and 21K19014), and partly supported by JST through the open innovation platform for industry-academia cocreation (COI-NEXT) Program (Grant Number JPMJPF2202).

■ REFERENCES

(1) Schirhagl, R.; Chang, K.; Loretz, M.; Degen, C. L. Nitrogen-Vacancy Centers in Diamond: Nanoscale Sensors for Physics and Biology. *Annu. Rev. Phys. Chem.* **2014**, *65*, 83−105.

(2) Nunn, N.; Torelli, M.; McGuire, G.; Shenderova, O. Nanodiamond: A High Impact Nanomaterial. *Current Opinion in Solid State and Materials Science.* **2017**, *21*, 1−9.

(3) Sotoma, S.; Epperla, C. P.; Chang, H. Diamond Nanothermometry. *ChemNanoMat* **2018**, *4*, 15−27.

(4) Ashfold, M. N. R.; Goss, J. P.; Green, B. L.; May, P. W.; Newton, M. E.; Peaker, C. V. Nitrogen in Diamond. *Chem. Rev.* **2020**, *120* (12), 5745−5794.

(5) Mzyk, A.; Sigaeva, A.; Schirhagl, R. Relaxometry with Nitrogen Vacancy (NV) Centers in Diamond. *Acc. Chem. Res.* **2022**, *55* (24), 3572−3580.

(6) Qureshi, S. A.; Hsiao, W. W.-W.; Hussain, L.; Aman, H.; Le, T.-N.; Rafique, M. Recent Development of Fluorescent Nanodiamonds for Optical Biosensing and Disease Diagnosis. *Biosensors* **2022**, *12* (12), 1181.

(7) Wu, Y.; Weil, T. Recent Developments of Nanodiamond Quantum Sensors for Biological Applications. *Adv. Sci.* **2022**, *9* (19), 1−19.

(8) Mochalin, V. N.; Shenderova, O.; Ho, D.; Gogotsi, Y. The Properties and Applications of Nanodiamonds. *Nat. Nanotechnol.* **2012**, *7* (1), 11−23.

(9) van der Laan, K.; Hasani, M.; Zheng, T.; Schirhagl, R. Nanodiamonds for In vivo Applications. *Small* **2018**, *14* (19), 1703838.

(10) Maze, J. R.; Stanwix, P. L.; Hodges, J. S.; Hong, S.; Taylor, J. M.; Cappellaro, P.; Jiang, L.; Dutt, M. V. G.; Togan, E.; Zibrov, A. S.; et al. Nanoscale Magnetic Sensing with an Individual Electronic Spin in Diamond. *Nature* **2008**, *455*, 644−647.

(11) Kucsko, G.; Maurer, P. C.; Yao, N. Y.; Kubo, M.; Noh, H. J.; Lo, P. K.; Park, H.; Lukin, M. D. Nanometre-Scale Thermometry in a Living Cell. *Nature* **2013**, *500*, 54−58.

(12) Neumann, P.; Jakobi, I.; Dolde, F.; Burk, C.; Reuter, R.; Waldherr, G.; Honert, J.; Wolf, T.; Brunner, A.; Shim, J. H.; et al. High-Precision Nanoscale Temperature Sensing Using Single Defects in Diamond. *Nano Lett.* **2013**, *13* (6), 2738−2742.

(13) Toyli, D. M.; de las Casas, C. F.; Christle, D. J.; Dobrovitski, V. V.; Awschalom, D. D. Fluorescence Thermometry Enhanced by the Quantum Coherence of Single Spins in Diamond. *Proc. Natl. Acad. Sci. U. S. A.* **2013**, *110* (21), 8417−8421.

(14) Fujisaku, T.; Tanabe, R.; Onoda, S.; Kubota, R.; Segawa, T. F.; So, F. T. K.; Ohshima, T.; Hamachi, I.; Shirakawa, M.; Igarashi, R. pH Nanosensor Using Electronic Spins in Diamond. *ACS Nano* **2019**, *13* (10), 11726−11732.

(15) Barnard, A. S. Self-Assembly in Nanodiamond Agglutinates. *J. Mater. Chem.* **2008**, *18* (34), 4038.

(16) Marcon, L.; Riquet, F.; Vicogne, D.; Szunerits, S.; Bodart, J.-F.; Boukherroub, R. Cellular and in vivo Toxicity of Functionalized Nanodiamond in Xenopus Embryos. *J. Mater. Chem.* **2010**, *20* (37), 8064.

(17) Nagl, A.; Hemelaar, S. R.; Schirhagl, R. Improving Surface and Defect Center Chemistry of Fluorescent Nanodiamonds for Imaging Purposes—a Review. *Anal. Bioanal. Chem.* **2015**, *407* (25), 7521−7536.

(18) Tsai, L.-W.; Lin, Y.-C.; Perevedentseva, E.; Lugovtsov, A.; Priezzhev, A.; Cheng, C.-L. Nanodiamonds for Medical Applications: Interaction with Blood in vitro and in vivo. *Int. J. Mol. Sci.* **2016**, *17* (7), 1111.

(19) Zhang, X.; Fu, C.; Feng, L.; Ji, Y.; Tao, L.; Huang, Q.; Li, S.; Wei, Y. PEGylation and PolyPEGylation of Nanodiamond. *Polymer* **2012**, *53* (15), 3178−3184.

(20) Wang, D.; Tong, Y.; Li, Y.; Tian, Z.; Cao, R.; Yang, B. PEGylated Nanodiamond for Chemotherapeutic Drug Delivery. *Diam. Relat. Mater.* **2013**, *36*, 26−34.

(21) Uthappa, U. T.; Arvind, O. R.; Sriram, G.; Losic, D.; Ho-Young-Jung; Kigga, M.; Kurkuri, M. D. Nanodiamonds and Their Surface Modification Strategies for Drug Delivery Applications. *J. Drug Delivery Sci. Technol.* **2020**, *60*, No. 101993.

(22) Jung, H.-S.; Neuman, K. C. Surface Modification of Fluorescent Nanodiamonds for Biological Applications. *Nanomaterials* **2021**, *11* (1), 153.

(23) Merz, V.; Lenhart, J.; Vonhausen, Y.; Ortiz-Soto, M. E.; Seibel, J.; Krueger, A. Zwitterion-Functionalized Detonation Nanodiamond with Superior Protein Repulsion and Colloidal Stability in Physiological Media. *Small* **2019**, *15*, 1901551.

(24) Terada, D.; Genjo, T.; Segawa, T. F.; Igarashi, R.; Shirakawa, M. Nanodiamonds for Bioapplications−Specific Targeting Strategies. *Biochim. Biophys. Acta - Gen. Subj.* **2020**, *1864* (2), No. 129354.

(25) Yetisgin, A. A.; Cetinel, S.; Zuvin, M.; Kosar, A.; Kutlu, O. Therapeutic Nanoparticles and Their Targeted Delivery Applications. *Molecules* **2020**, *25* (9), 2193.

(26) Zou, Y.; Ito, S.; Yoshino, F.; Suzuki, Y.; Zhao, L.; Komatsu, N. Polyglycerol Grafting Shields Nanoparticles from Protein Corona Formation to Avoid Macrophage Uptake. *ACS Nano* **2020**, *14* (6), 7216−7226.

(27) Rafiee, Z.; Omidi, S. Modification of Carbon-Based Nanomaterials by Polyglycerol: Recent Advances and Applications. *RSC Adv.* **2021**, *12* (1), 181−192.

(28) Gref, R.; Domb, A.; Quellec, P.; Blunk, T.; Müller, R. H.; Verbavatz, J. M.; Langer, R. The Controlled Intravenous Delivery of Drugs Using PEG-Coated Sterically Stabilized Nanospheres. *Adv. Drug Delivery Rev.* **1995**, *16* (2−3), 215−233.

(29) Kenausis, G. L.; Vörös, J.; Elbert, D. L.; Huang, N.; Hofer, R.; Ruiz-Taylor, L.; Textor, M.; Hubbell, J. a.; Spencer, N. D. Poly(L-Lysine)-*g*-Poly(Ethylene Glycol) Layers on Metal Oxide Surfaces: Attachment Mechanism and Effects of Polymer Architecture on Resistance to Protein Adsorption. *J. Phys. Chem. B* **2000**, *104* (14), 3298−3309.

(30) Ong, S. Y.; Chipaux, M.; Nagl, A.; Schirhagl, R. Shape and Crystallographic Orientation of Nanodiamonds for Quantum Sensing. *Phys. Chem. Chem. Phys.* **2017**, *19* (17), 10748−10752.

(31) Reineck, P.; Trindade, L. F.; Havlik, J.; Stursa, J.; Heffernan, A.; Elbourne, A.; Orth, A.; Capelli, M.; Cigler, P.; Simpson, D. A.; et al. Not All Fluorescent Nanodiamonds Are Created Equal: A Comparative Study. *Part. Part. Syst. Charact.* **2019**, *36* (3), 1900009.

(32) Eldemrdash, S.; Thalassinos, G.; Alzahrani, A.; Sun, Q.; Walsh, E.; Grant, E.; Abe, H.; Greaves, T. L.; Ohshima, T.; Cigler, P.; et al.

Fluorescent HPHT Nanodiamonds Have Disk- and Rod-like Shapes. *Carbon* **2023**, *206*, 268−276.
(33) Kawaguchi, S.; Imai, G.; Suzuki, J.; Miyahara, A.; Kitano, T.; Ito, K. Aqueous Solution Properties of Oligo- and Poly(Ethylene Oxide) by Static Light Scattering and Intrinsic Viscosity. *Polymer* **1997**, *38* (12), 2885−2891.
(34) Rossetti, F. F.; Reviakine, I.; Csúcs, G.; Assi, F.; Vörös, J.; Textor, M. Interaction of Poly(L-Lysine)-g-Poly(Ethylene Glycol) with Supported Phospholipid Bilayers. *Biophys. J.* **2004**, *87* (3), 1711−1721.
(35) Tainaka, K.; Murakami, T. C.; Susaki, E. A.; Shimizu, C.; Saito, R.; Takahashi, K.; Hayashi-Takagi, A.; Sekiya, H.; Arima, Y.; Nojima, S.; et al. Chemical Landscape for Tissue Clearing Based on Hydrophilic Reagents. *Cell Rep.* **2018**, *24*, 2196−2210.
(36) Schindelin, J.; Arganda-Carreras, I.; Frise, E.; Kaynig, V.; Longair, M.; Pietzsch, T.; Preibisch, S.; Rueden, C.; Saalfeld, S.; Schmid, B.; et al. Fiji: An Open-Source Platform for Biological-Image Analysis. *Nat. Methods* **2012**, *9* (7), 676−682.
(37) Chung, P.-H.; Perevedentseva, E.; Tu, J.-S.; Chang, C. C.; Cheng, C.-L. Spectroscopic Study of Bio-Functionalized Nanodiamonds. *Diam. Relat. Mater.* **2006**, *15* (4−8), 622−625.
(38) Terada, D.; Segawa, T. F.; Shames, A. I.; Onoda, S.; Ohshima, T.; Ōsawa, E.; Igarashi, R.; Shirakawa, M. Monodisperse Five-Nanometer-Sized Detonation Nanodiamonds Enriched in Nitrogen-Vacancy Centers. *ACS Nano* **2019**, *13* (6), 6461−6468.
(39) Petit, T.; Puskar, L. FTIR Spectroscopy of Nanodiamonds: Methods and Interpretation. *Diam. Relat. Mater.* **2018**, *89*, 52−66.
(40) Wrobel, N.; Schinkinger, M.; Mirsky, V. M. A Novel Ultraviolet Assay for Testing Side Reactions of Carbodiimides. *Anal. Biochem.* **2002**, *305* (2), 135−138.
(41) Nojima, Y.; Iguchi, K.; Suzuki, Y.; Sato, A. The PH-Dependent Formation of PEGylated Bovine Lactoferrin by Branched Polyethylene Glycol (PEG)-N-Hydroxysuccinimide (NHS) Active Esters. *Biol. Pharm. Bull.* **2009**, *32* (3), 523−526.
(42) Sofia, S. J.; Premnath, V.; Merrill, E. W. Poly(Ethylene Oxide) Grafted to Silicon Surfaces: Grafting Density and Protein Adsorption. *Macromolecules* **1998**, *31* (15), 5059−5070.
(43) Walkey, C. D.; Olsen, J. B.; Guo, H.; Emili, A.; Chan, W. C. W. Nanoparticle Size and Surface Chemistry Determine Serum Protein Adsorption and Macrophage Uptake. *J. Am. Chem. Soc.* **2012**, *134* (4), 2139−2147.
(44) Vaijayanthimala, V.; Cheng, P.; Yeh, S.; Liu, K.; Hsiao, C.; Chao, J.; Chang, H. The Long-Term Stability and Biocompatibility of Fluorescent Nanodiamond as an in vivo Contrast Agent. *Biomaterials* **2012**, *33* (31), 7794−7802.
(45) Yasukawa, M.; Tanaka, Y.; Takahashi, T.; Shibuya, M.; Mishima, S.; Matsuyama, H. Effect of Molecular Weight of Draw Solute on Water Permeation in Forward Osmosis Process. *Ind. Eng. Chem. Res.* **2015**, *54* (33), 8239−8246.
(46) Alexander, S. Adsorption of Chain Molecules With a Polar Head. A Scaling Description. *J. Phys. (Paris)* **1977**, *38* (8), 983−987.
(47) de Gennes, P. G. Conformations of Polymers Attatched to an Interface. *Macromolecules* **1980**, *13* (19), 1069−1075.
(48) Tockary, T. A.; Osada, K.; Chen, Q.; Machitani, K.; Dirisala, A.; Uchida, S.; Nomoto, T.; Toh, K.; Matsumoto, Y.; Itaka, K.; et al. Tethered PEG Crowdedness Determining Shape and Blood Circulation Profile of Polyplex Micelle Gene Carriers. *Macromolecules* **2013**, *46* (16), 6585−6592.
(49) Chen, W. Y.; Zheng, J. X.; Cheng, S. Z. D.; Li, C. Y.; Huang, P.; Zhu, L.; Xiong, H.; Ge, Q.; Guo, Y.; Quirk, R. P.; et al. Onset of Tethered Chain Overcrowding. *Phys. Rev. Lett.* **2004**, *93* (2), 028301−1.
(50) Adumeau, L.; Genevois, C.; Roudier, L.; Schatz, C.; Couillaud, F.; Mornet, S. Impact of Surface Grafting Density of PEG Macromolecules on Dually Fluorescent Silica Nanoparticles Used for the in Vivo Imaging of Subcutaneous Tumors. *Biochim. Biophys. Acta* **2017**, *1861* (6), 1587−1596.

https://doi.org/10.1021/acs.langmuir.3c03988
Langmuir XXXX, XXX, XXX−XXX